Electronic Supplementary Material (ESI) for Inorganic Chemistry Frontiers.

Post-synthetic Modification of Bis-iron(III)-μ-oxo-porphyrin Prisms to Enhance Oxygen Reduction Electrocatalysis

Daoyang Zhang[a], Lauren E. Rosch[a], Matthew R. Crawley[a], and Timothy R. Cook*[, a]

[a]Department of Chemistry, University at Buffalo, The State University of New York, Buffalo, New York 14260, United States

Email: trcook@buffalo.edu

Table of Contents

Spectroscopic characterization

^{1}H NMR spectroscopy

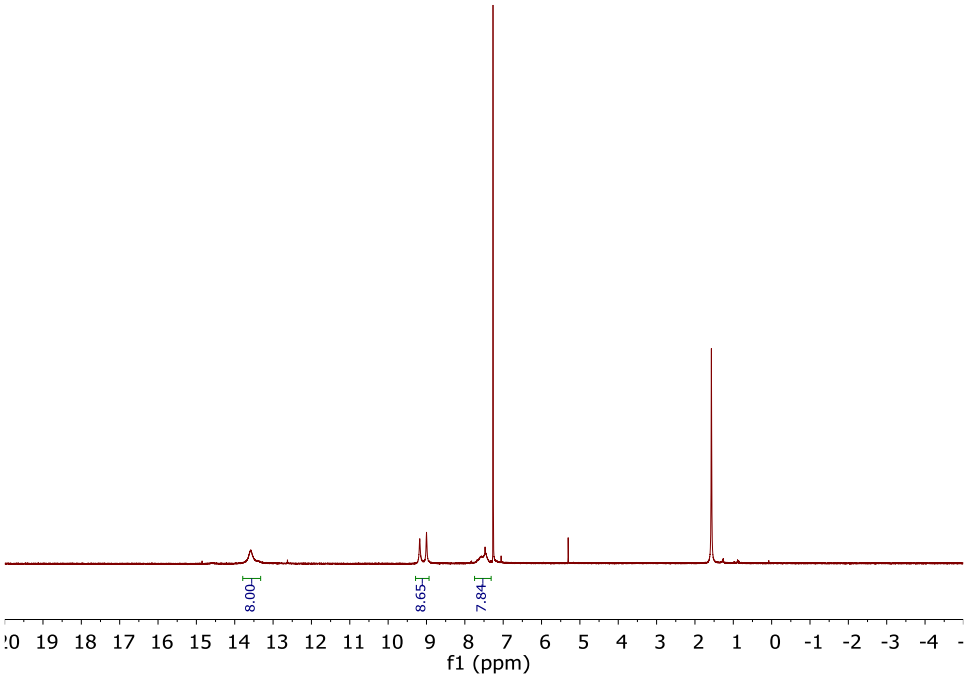

Figure S1. ^{1}H NMR spectrum of Fe_2O TPyP ((CDCl$_3$, 500 MHz, 298 K).

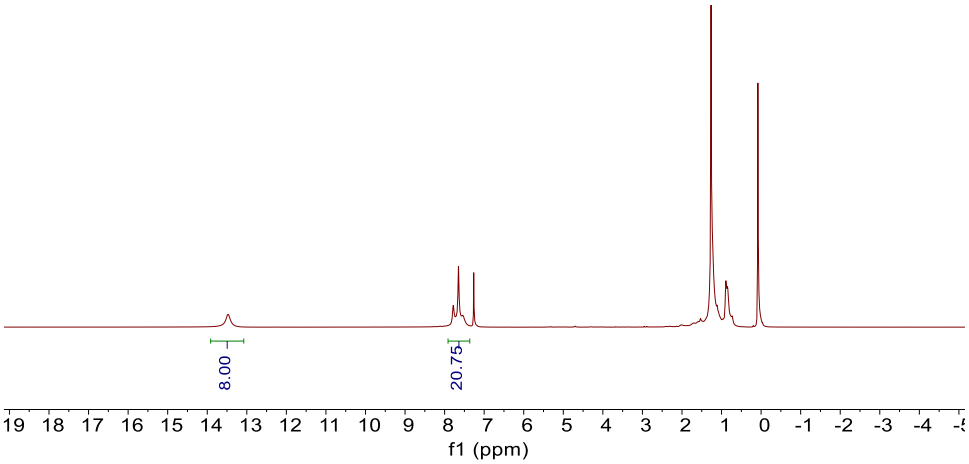

Figure S2. ^{1}H NMR spectrum of Fe_2O TPP (CDCl$_3$, 500 MHz, 298 K).

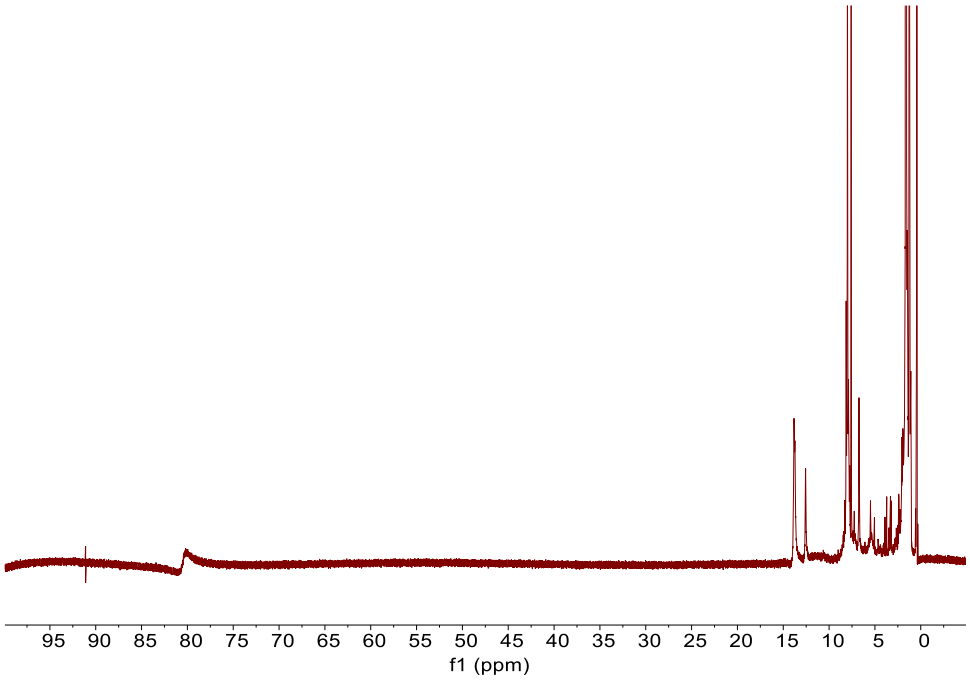

Figure S3. ^{1}H NMR spectrum of FeTPPCl ($CDCl_3$, 500 MHz, 298 K).

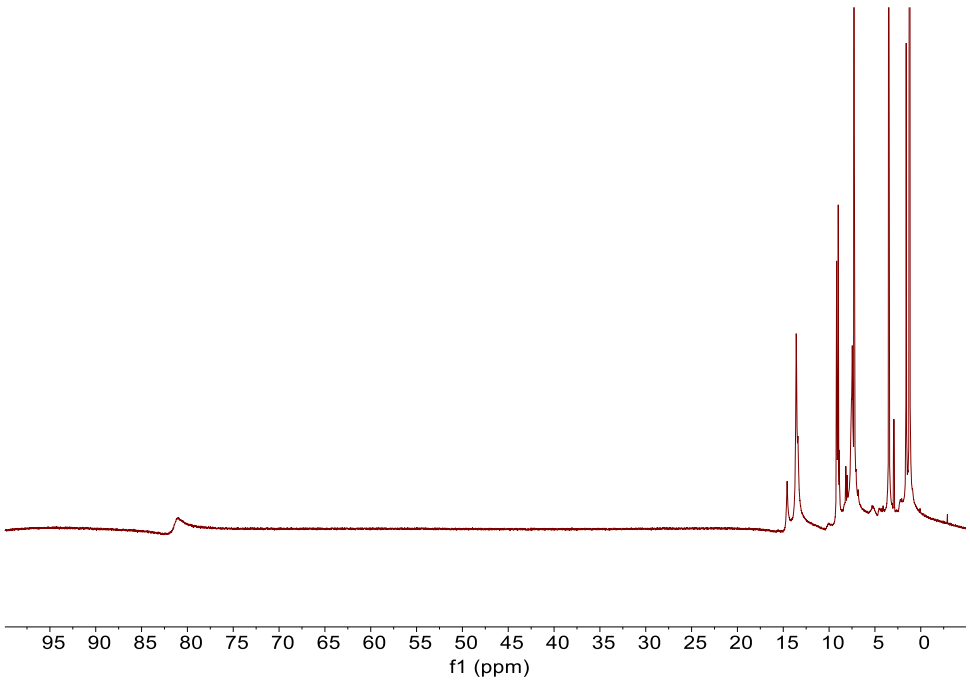

Figure S4. ^{1}H NMR spectrum of FeTPyPCl ($CDCl_3$, 500 MHz, 298 K).

DOSY

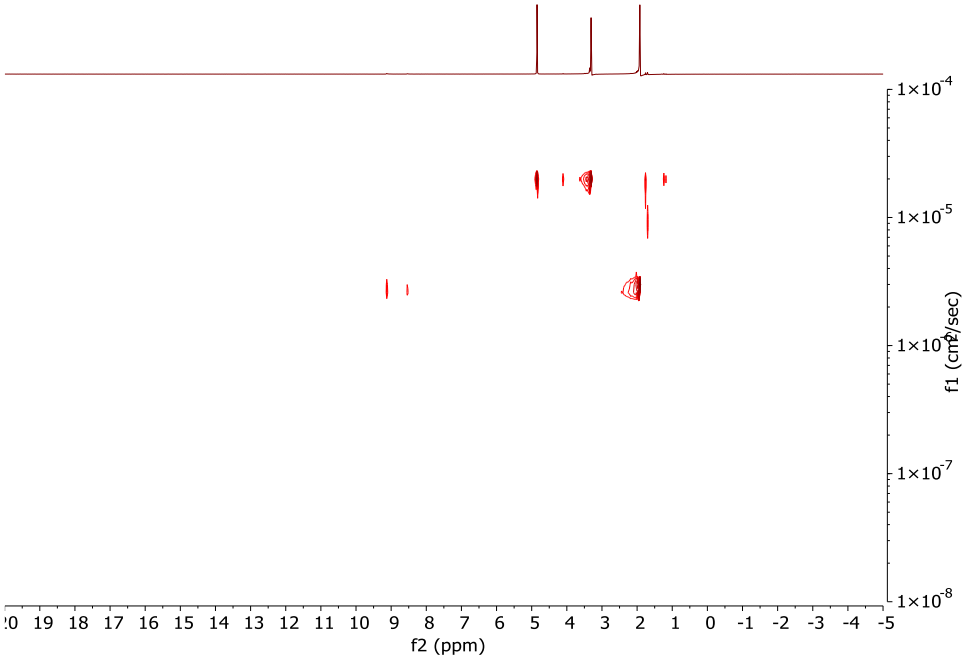

Figure S5. DOSY spectrum of Fe_2O Rhoxo prism (CD_3OD, 500 MHz, 298 K).

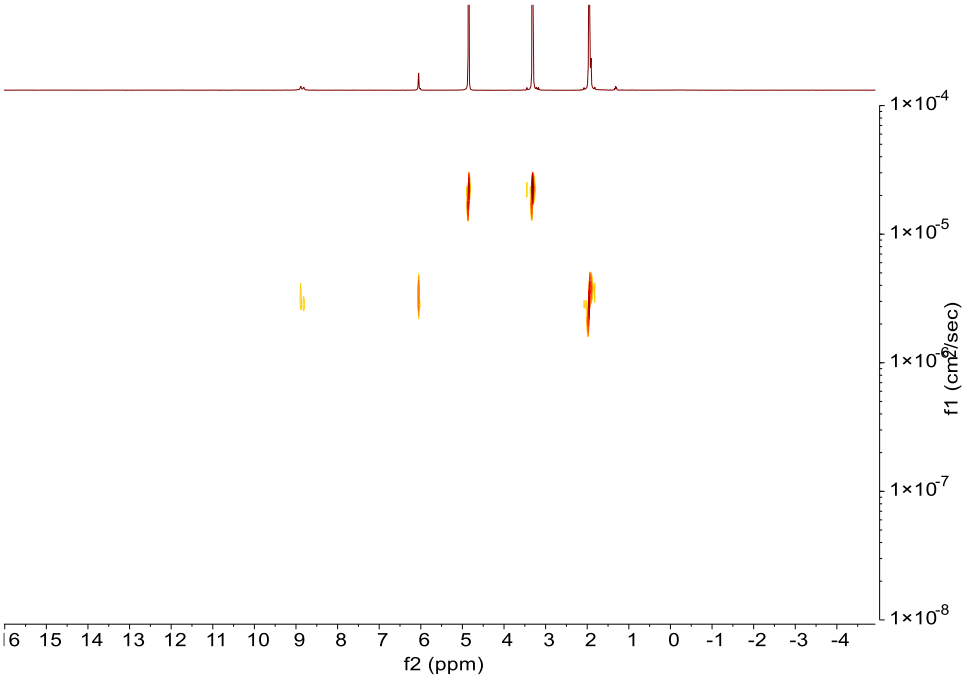

Figure S6. DOSY spectrum of Fe_2O Rh-benzo prism (CD_3OD, 500 MHz, 298 K).

VT-NMR

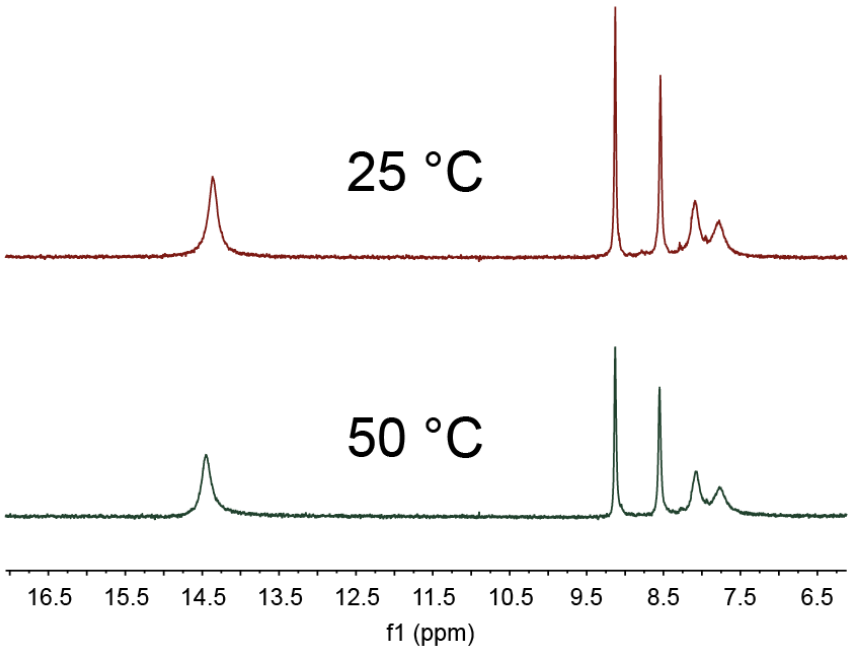

Figure S7. VT NMR of Fe_2O Rhoxo prism. (CD_3OD, 500 MHz).

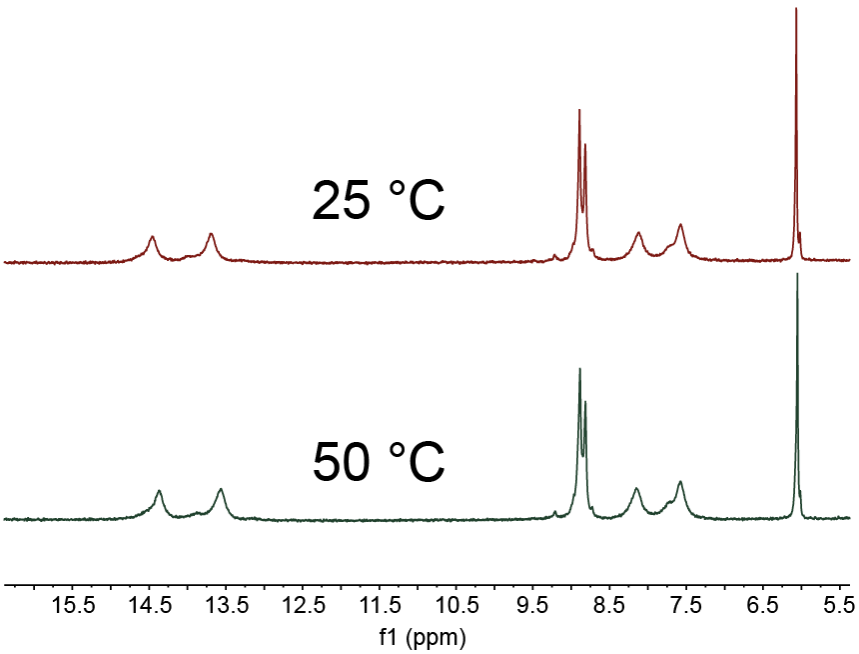

Figure S8. VT NMR OF Fe_2O Rh-benzo prism. (CD_3OD, 500 MHz).

Mass-spectrometry

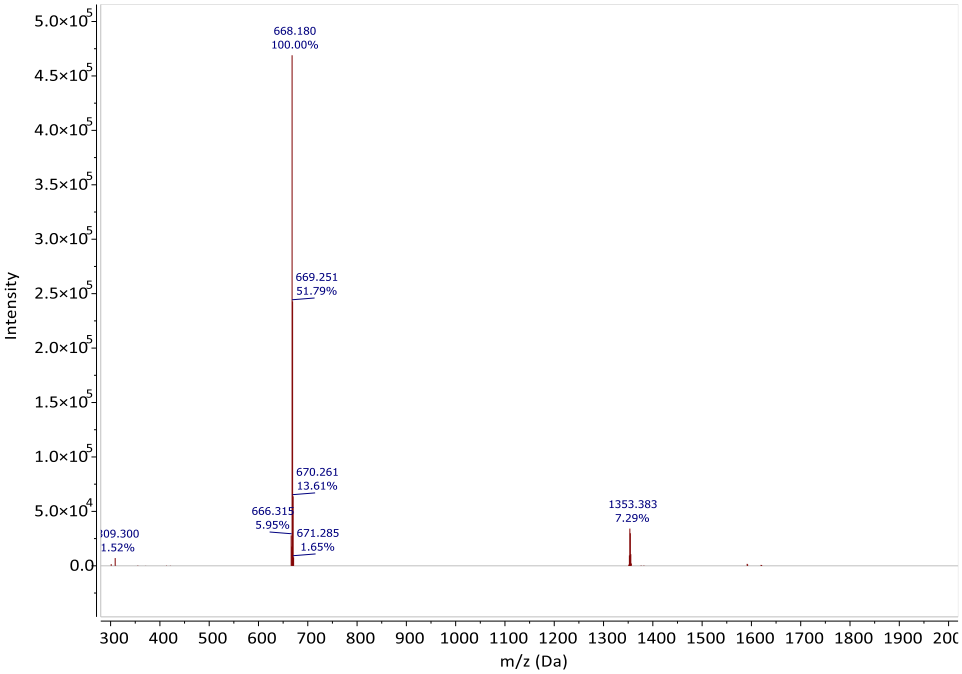

Figure S9. LTQ-MS of $FeTPhP_2O$, m/z = 1353.383 was attributed to the $M+H^+$.

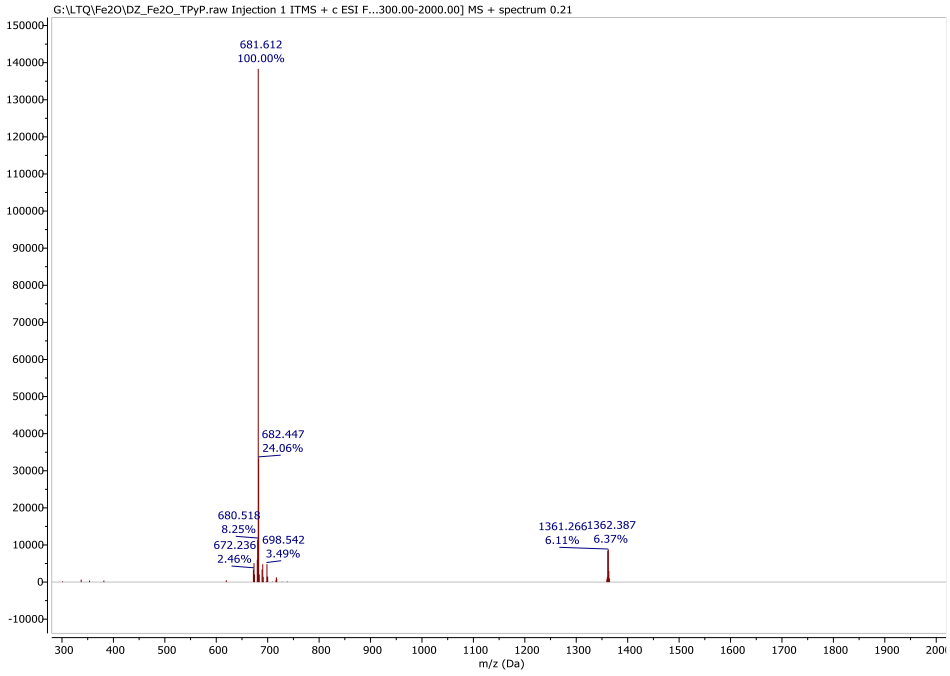

Figure S10. LTQ-MS of $FeTPyP_2O$, m/z = 1361.226 was attributed to the $M+H^+$.

Electrochemical measurements

Cyclic voltammetry:

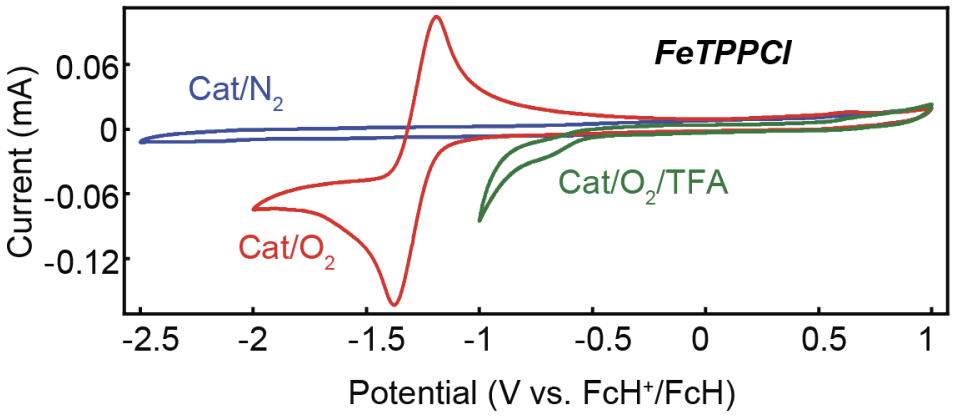

Figure S11. CV of FeTPPCl under homogeneous condition. 0.1 mM prism. All in DMF with 100 mM $TBAPF_6$. Scan rate: 100 mV s^{-1}.

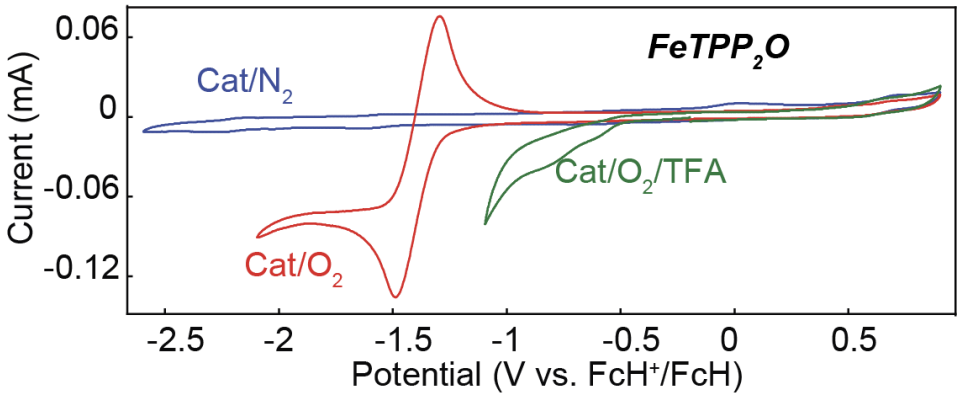

Figure S12. CV of $FeTPP_2O$ under homogeneous condition. 0.1 mM prism. All in DMF with 100 mM $TBAPF_6$. Scan rate: 100 mV s^{-1}.

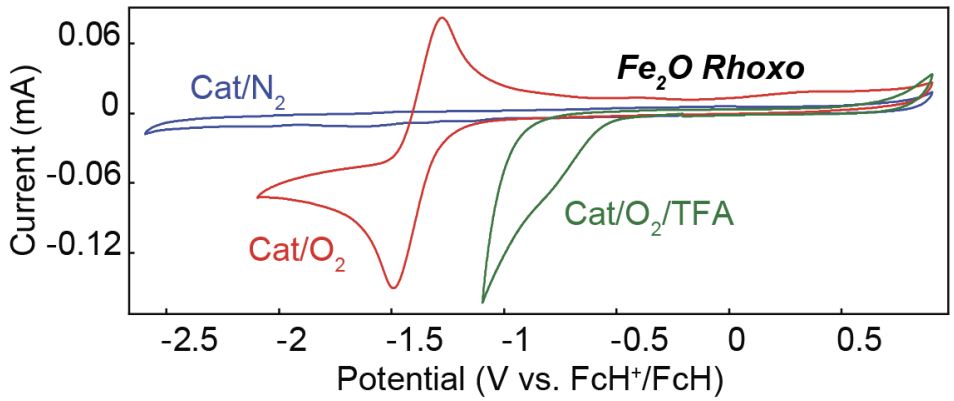

Figure S13. CV of Fe_2O Rhoxo under homogeneous condition. 0.1 mM prism. All in DMF with 100 mM $TBAPF_6$. Scan rate: 100 mV s^{-1}.

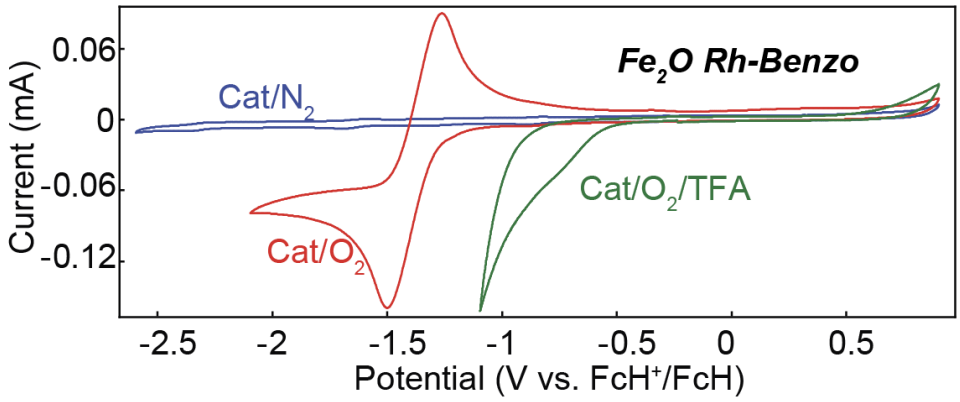

Figure S14. CV of Fe_2O Rh-benzo under homogeneous condition. 0.1 mM prism. All in DMF with 100 mM $TBAPF_6$. Scan rate: 100 mV s^{-1}.

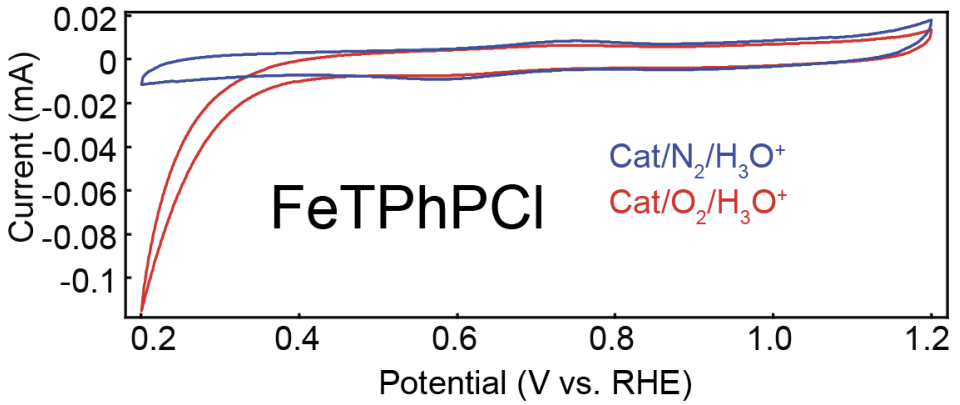

Figure S15. CV under heterogeneous conditions. N_2 atmosphere (blue); O_2atmosphere (red) FeTPPCl was immobilized in Nafion inks with carbon black and immersed in 0.5 M H_2SO_4. Scan rate: 100 mV s^{-1}.

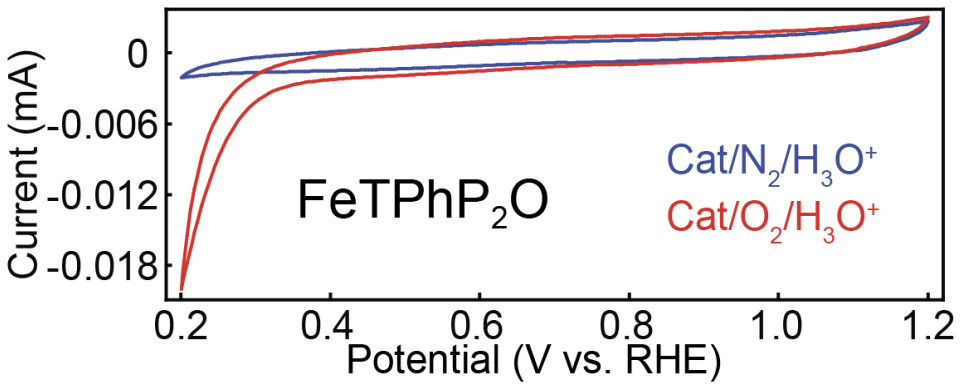

Figure S16. CV under heterogeneous conditions. N_2 atmosphere (blue); O_2atmosphere (red) $FeTPP_2O$ was immobilized in Nafion inks with carbon black and immersed in 0.5 M H_2SO_4. Scan rate: 100 mV s^{-1}.

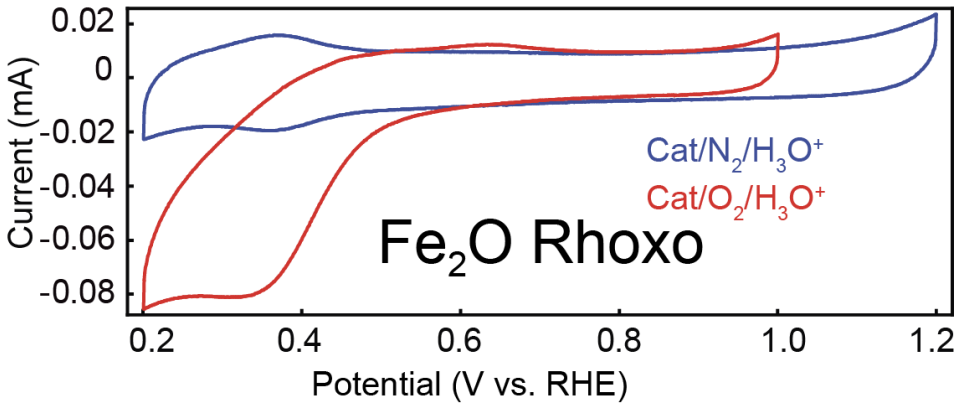

Figure S17. CV under heterogeneous conditions. N_2 atmosphere (blue); O_2atmosphere (red) Fe_2O Rhoxo Prism was immobilized in Nafion inks with carbon black and immersed in 0.5 M H_2SO_4. Scan rate: 100 mV s^{-1}.

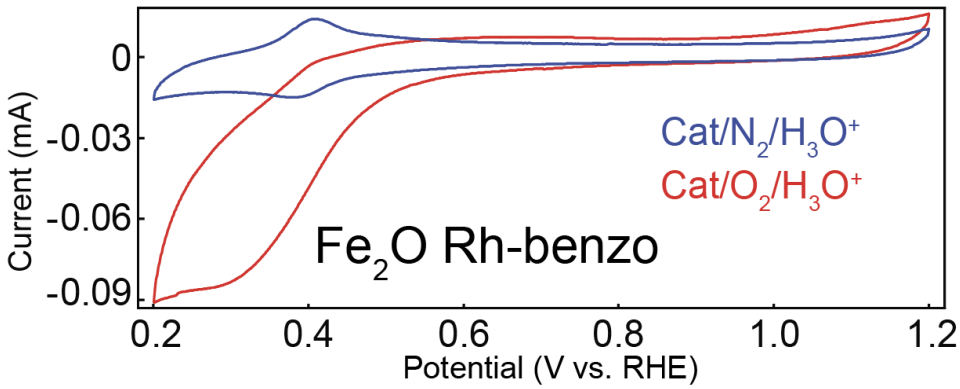

Figure S18. CV under heterogeneous conditions. N_2 atmosphere (blue); O_2atmosphere (red) Fe_2O Rh-benzo Prism was immobilized in Nafion inks with carbon black and immersed in 0.5 M H_2SO_4. Scan rate: 100 mV s^{-1}.

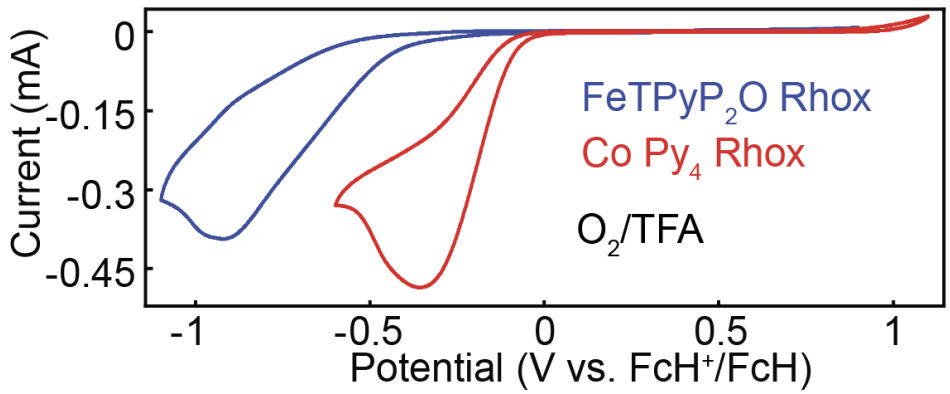

Figure S19. Catalytic CV under homogeneous condition. 0.1 mM prism, O_2 atmosphere, 100 mM TFA. All in acetonitrile with 100 mM $TBAPF_6$. Scan rate: 100 mV s^{-1}.

Linear sweep voltammetry

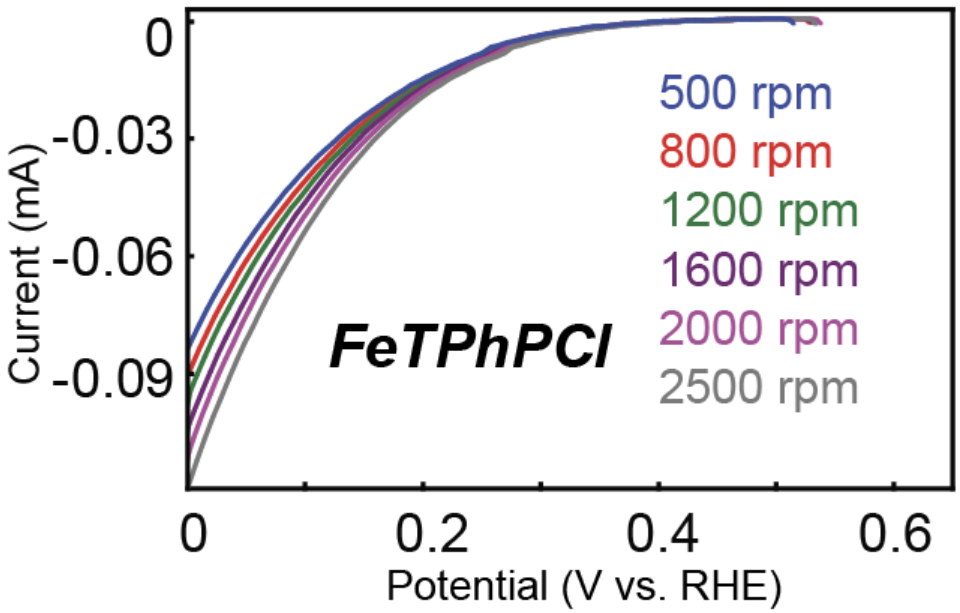

Figure S20. LSV of FeTPPCl under heterogeneous conditions with different rotation rates. FeTPPCl was immobilized in Nafion inks with carbon black and immersed in 0.5 M H_2SO_4. Scan rate: 20 mV s^{-1}.

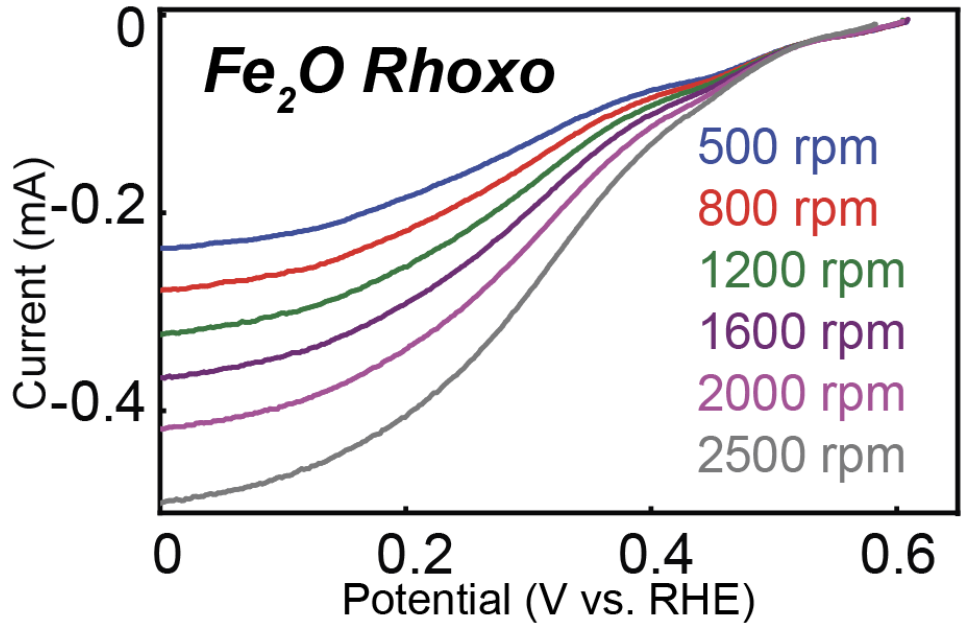

Figure S21. LSV of $(FeTPhP)_2O$ under heterogeneous conditions with different rotation rates. $(FeTPhP)_2O$ was immobilized in Nafion inks with carbon black and immersed in 0.5 M H_2SO_4. Scan rate: 20 mV s^{-1}.

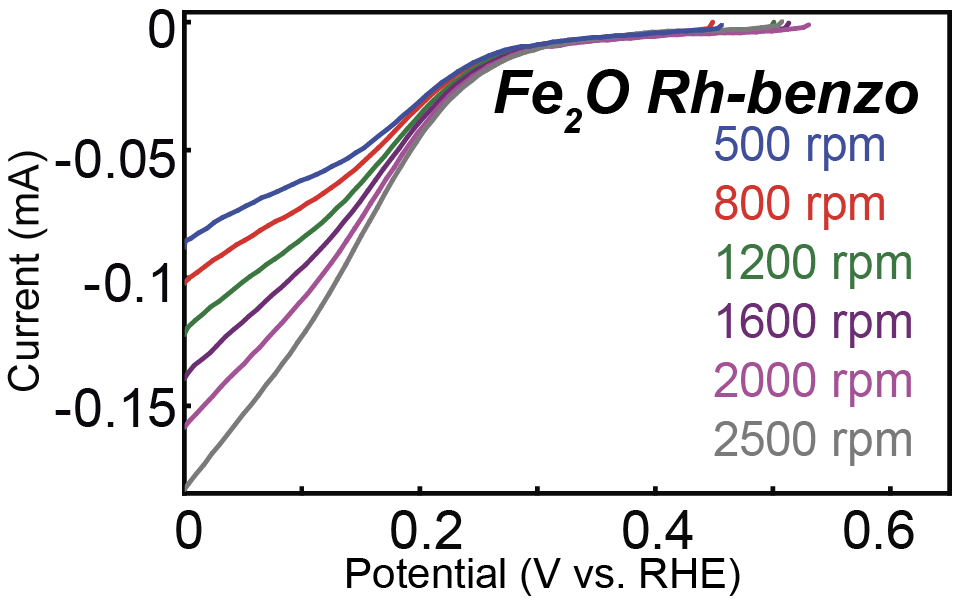

Figure S22. LSV of Fe_2O Rhoxo under heterogeneous conditions with different rotation rates. Fe_2O Rhoxo was immobilized in Nafion inks with carbon black and immersed in 0.5 M H_2SO_4. Scan rate: 20 mV s^{-1}.

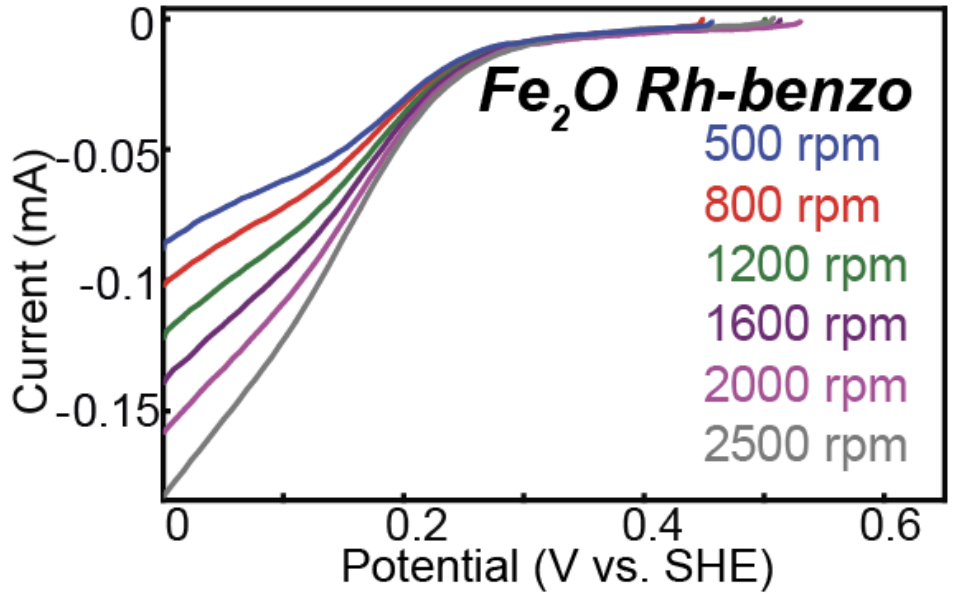

Figure S23. LSV of Fe_2O Rh-benzo under heterogeneous conditions with different rotation rates. Fe_2O Rh-benzo was immobilized in Nafion inks with carbon black and immersed in 0.5 M H_2SO_4. Scan rate: 20 mV s^{-1}.

Koutecký-Levich analysis

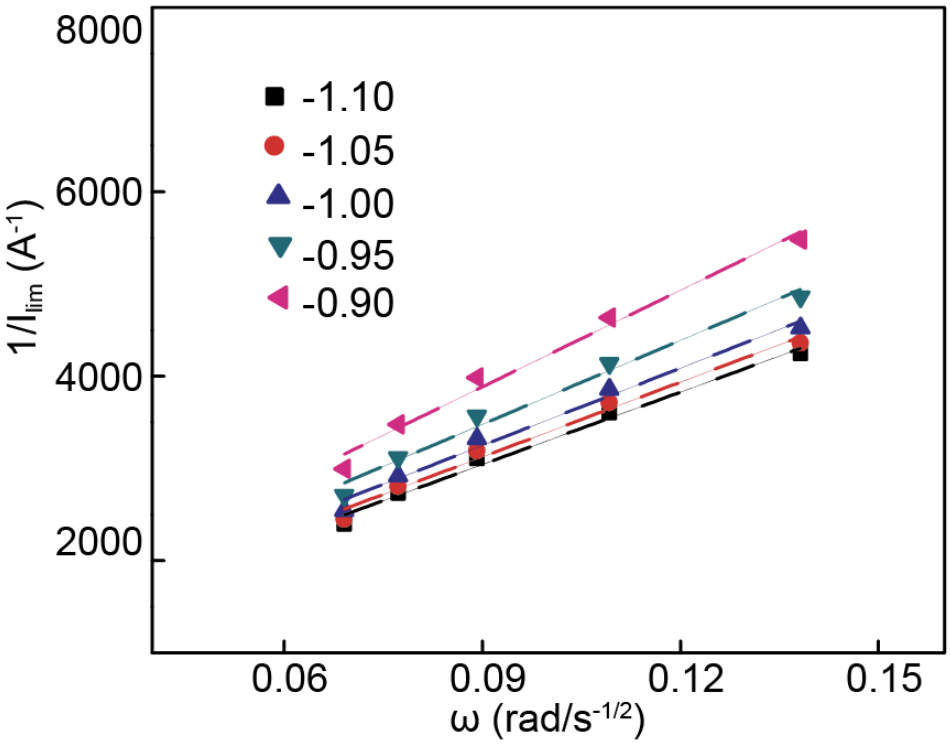

Figure S24. Koutecký-Levich plots of Fe_2O Rhoxo Prism

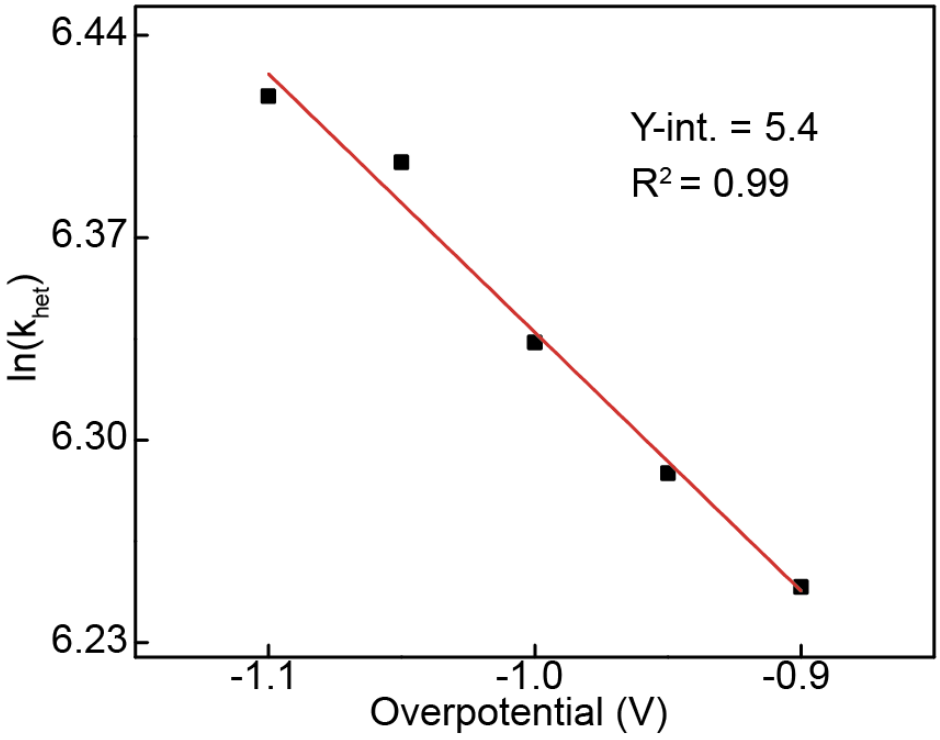

Figure S25. Plot of $\ln(k_{het})$ vs. overpotential for the Fe_2O Rhoxo Prism. The y-intercept of this plot is $\ln(k_s)$. The k_s value was calculated as 2.6×10^2

Koutecký-Levich Analysis and Determination of K_s

Figure S24 was constructed by collecting and plotting current response data at specific overpotentials across a range of rotation rates.

For the analysis using Equations S1-S5, i_{lim} is the limiting current taken from the plateau of the voltammograms (amps) shown in Figure S21, ω is the rotation rate (rad/s), i_K is the kinetically limited current (amps), n is the number of electrons transferred as determined from Equation S4, F is the Faraday Constant, k_{het} is the heterogeneous electron transfer rate constant ($M^{-1}s^{-1}$ due to the Γ_{cat} term), $[O_2]$ is the concentration of O_2 dissolved in solution (mol/L), and Γ_{cat} is the number of active catalyst sites per surface area (mol/cm^2). For Equations S3A and S3B, η is the overpotential (V), α is the transfer coefficient, k_s is the standard rate constant (here in $M^{-1}s^{-1}$).

We calculated a Γ_{cat} based on our catalyst loading in the catalyst ink. An assumption was made that all moles of catalyst added were active. Any inactive or inaccessible catalytic sites would result in our calculated k_{het} and k_s values being lower than their actual values. Thus, our values are a lower limit and actual catalyst kinetics must be either equal or better.

From the plot in Figure S24, values for i_k were extracted as the Y-intercepts for each overpotential trace. These values were then used along with Equation S2B to solve for values of k_{het} at each overpotential. These k_{het} values were used to construct Figure S25 from which a k_s value could be extracted from the Y-intercept using Equation S3B

From this plot, the Y-intercepts for the traces corresponding to each overpotential were determined. . Extract the Y-intercept as $1/i_k$, then use Equation S2 to obtain the value k_{het}. Finally, plot the $\ln(k_{het})$ with overpotential as shown in Figure S25, to obtain the Y-intercept as the standard rate constant values k_s.[1]

$$\frac{1}{i_{lim}} = \omega^{-1/2} + \frac{1}{i_k} \qquad \text{Equation S1}$$

$$i_k = nFAk_{het}[O_2]\Gamma_{cat} \qquad \text{Equation S2A}$$

$$k_{het} = \frac{i_k}{nFA[O_2]\Gamma_{cat}} \qquad \text{Equation S2B}$$

$$k_{het} = k_s e^{\frac{-a\eta}{RT}} \qquad \text{Equation S3A}$$

$$\ln(k_{het}) = \frac{-a}{RT}\eta - \ln(k_s) \qquad \text{Equation S3B}$$

$$n = 4 - 2\left(\frac{\%H_2O_2}{100}\right) \qquad \text{Equation S4}$$

$$\%H_2O_2 = \frac{\frac{2i_{ring}}{N}}{i_{disk} + \frac{i_{ring}}{N}} \times 100 \qquad \text{Equation S5.}$$

UV-vis spectroelectrochemistry:

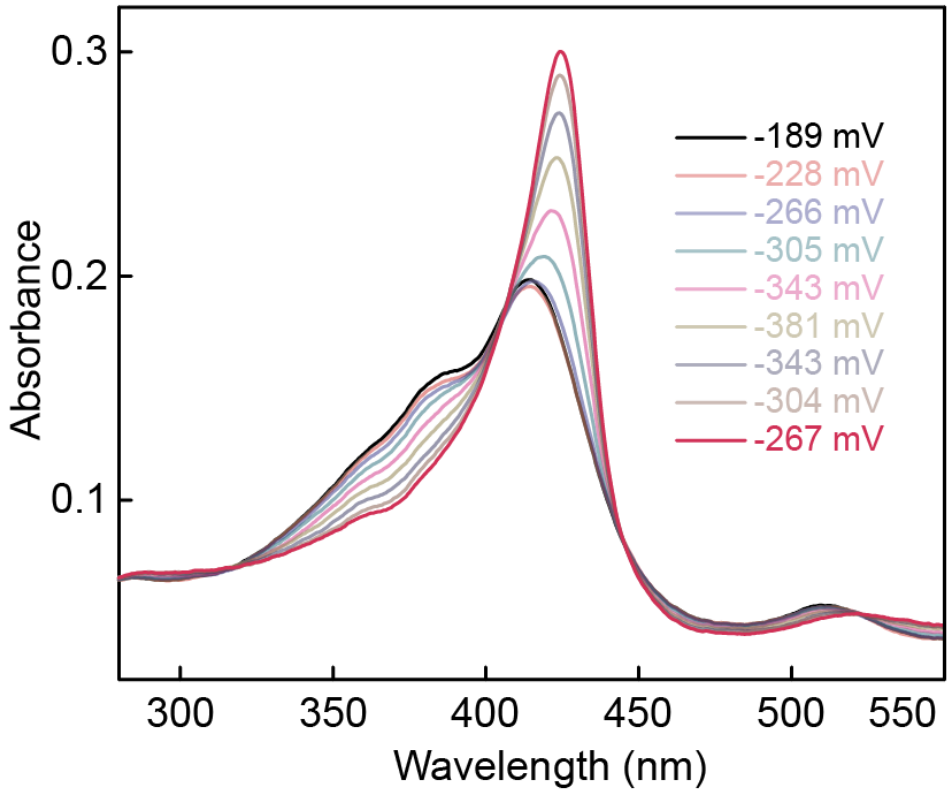

Figure S26. UV-vis spectroelectrochemistry of $FeTPP_2O$. 0.01 mmol prism, N_2 atmosphere, 100 mM TFA. Acetonitrile with 100 mM $TBABF_4$.

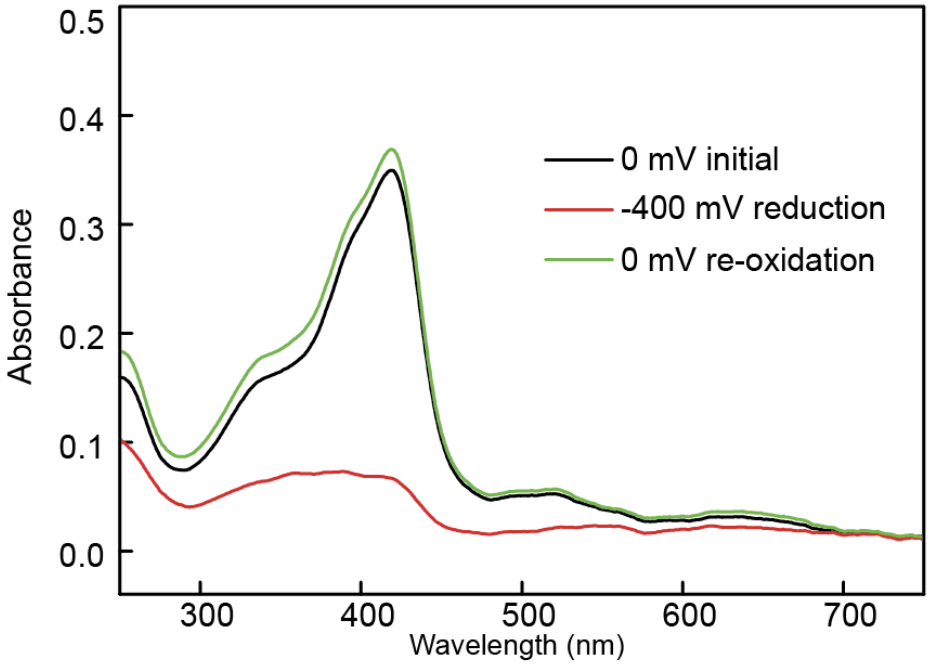

Figure S27. UV-vis spectroelectrochemistry of Fe_2O Rhoxo. 0.01 mmol prism, N_2 atmosphere, 100 mM TFA. Acetonitrile with 100 mM $TBABF_4$.

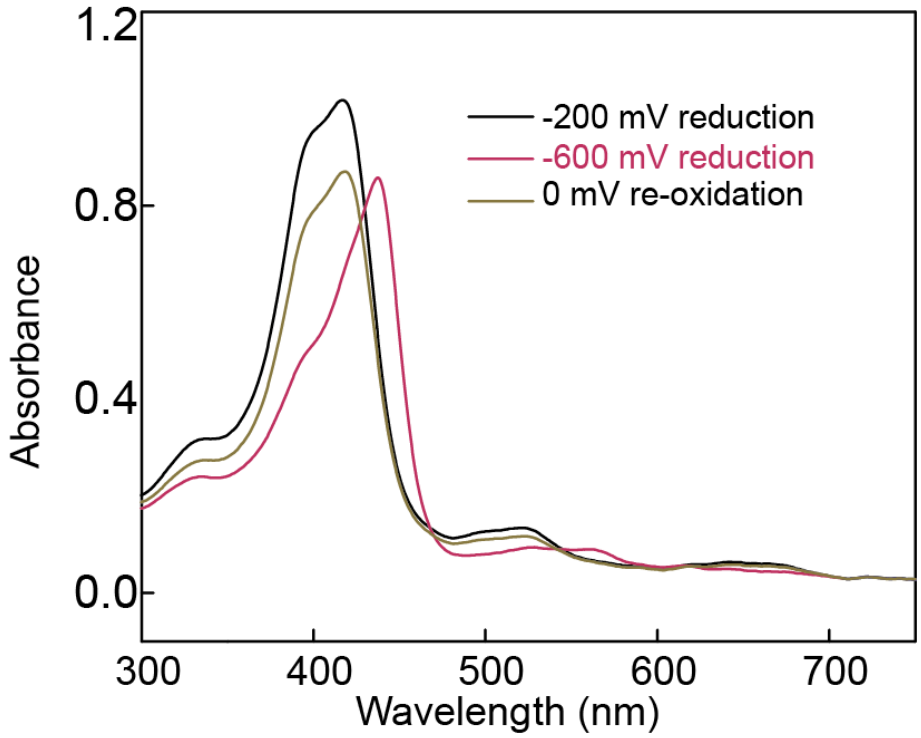

Figure S28. UV-vis spectroelectrochemistry of Fe_2O Rhoxo. 0.016 mmol prism, N_2 atmosphere, 100 mM TFA. DMF with 100 mM $TBABF_4$.

Computational:

The structures of **Fe_2O Rhoxo** and **Fe_2O Rh-benzo** were optimized using ORCA 5.0.3,[2] at the r^2SCAN-3c level of theory from Grimme with def2-mTZVPP basis set.[3] The solvent effects of methanol were treated using the conductor-like polarizable continuum model (CPCM). For the purposes of geometry optimization, we have treated the Fe_2O prisms as spin singlets. The spin-states of the Fe_2O prisms have not been rigorously determined in this work; however, given the NMR spectra, as well as the literature reports of strong antiferromagnetic coupling in Fe(III)–O–Fe(III) systems,[4] it is reasonable to treat them as such.

To address the possibility of so called "bowtie" complexes, computationally derived models were used. The structure of the **Zn Rh-benzo** was optimized at the r^2scan level of theory with the def2-mTZVPP basis set. The diamagnetic Zn analogue was used to expedite the geometry optimization by alleviating any ambiguity in spin state. Using the optimized geometry as the starting point one of the porphyrin rings and three of the four clips were removed and the remaining clip was rotated about the Rh—N bond vector. The clip was rotated to be parallel with the plane of the porphyrin, moving the second Rh center to its most proximal position to the adjacent pyridyl ring. The Rh-N distance was found to be ~7.3 Å in comparison with the pyridyl N-N distance of ~10.9 Å. These findings suggest that the angularity and Rh—Rh distance of the Rh-benzo precludes the formation of "bowties" with TPyP-based donors as shown in Figure S29.

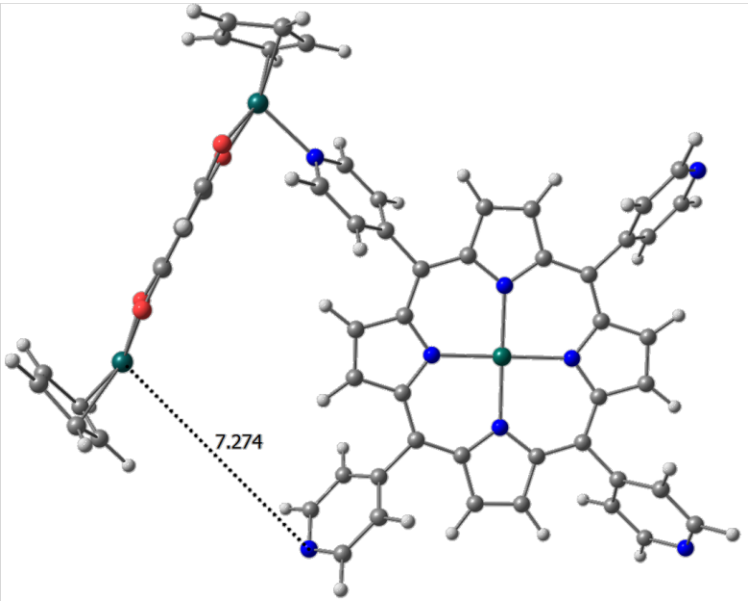

Figure S29. Optimized structure of potential bowtie structure with metallo tetrapyridyl porphyrin and Rh-benzo clip.

1. Zhang, J., *PEM Fuel Cell Electrocatalysts and Catalyst Layers: Fundamentals and Applications*. Springer London: 2008.
2. Neese, F.; Wennmohs, F.; Becker, U.; Riplinger, C., The ORCA quantum chemistry program package. *The Journal of Chemical Physics* **2020,** *152* (22), 224108.
3. Grimme, S.; Hansen, A.; Ehlert, S.; Mewes, J.-M., r2SCAN-3c: A "Swiss army knife" composite electronic-structure method. *The Journal of Chemical Physics* **2021,** *154* (6), 064103.
4. Abdullin, D.; Fleck, N.; Klein, C.; Brehm, P.; Spicher, S.; Lützen, A.; Grimme, S.; Schiemann, O., Synthesis of μ2-Oxo-Bridged Iron(III) Tetraphenylporphyrin–Spacer–Nitroxide Dimers and their Structural and Dynamics Characterization by using EPR and MD Simulations. *Chem. - Eur. J.* **2019,** *25* (10), 2586-2596.